energies

MDPI

Article

Optimization of Acid Fracturing Process for Carbonate Reservoirs in Daniudi Gas Field

Yongchun Zhang [1,2,*], Haijun Mao [3,4,*], Hao Zhang [1], Yueli Li [2], Yanfang Jiang [2] and Jiarui Li [2]

[1] Chengdu University of Technology, Chengdu 610059, China
[2] Petroleum Engineering Technology Research Institute of Sinopec North China E & P Company, Zhengzhou 450006, China
[3] Wuhan Institute of Rock and Soil Mechanics, Chinese Academy of Sciences, Wuhan 430071, China
[4] State Key Laboratory of Geomechanics and Geotechnical Engineering, Chinese Academy of Sciences, Wuhan 430071, China
* Correspondence: hbjzyc@126.com (Y.Z.); hjmao@whrsm.ac.cn (H.M.)

Abstract: The Daniudi gas field is located in the Ordos Basin's northern section of the Yishan slope. The intertidal–subtidal depositional environment dominates the lithology of the Ma55 sub-member, resulting in a stable, thick-layered dark gray–gray–black limestone and lime dolomite. The stratum is stable laterally as well as dolomite, with an average thickness of 26.8 m. Fractures, dissolution expansion pores, and inter-crystalline dissolved pores are the primary reservoir space kinds, with a minor number of karst caves and fractures generated as well. The main distribution ranges for porosity and permeability are 1–8 percent and 0.01–1 mD, respectively. Low porosity, tightness, and ultra-low permeability are common characteristics, and a single well typically has no natural productivity. Production stimulation technologies like pre-fluid acid fracturing, compound sand addition acid fracturing, and multi-stage injection + temporary plugging volumetric acid fracturing have been gradually optimized using the horizontal well development method, and breakthroughs in the development of tight and low-permeability carbonate rock reservoirs have been made. However, the conditions of different types of reservoirs are quite different, and the acid fracturing process is not matched and imperfect, resulting in large differences in the productivity of different horizontal wells after fracturing, as well as a high proportion of low-yield wells, which cannot meet the needs of cost-effective and effective development of this type of gas reservoir. In light of the aforementioned issues, a series of laboratory tests have been carried out to explore the stimulation effects of acid fracturing on different types of reservoirs and to optimize the acid fracturing process in the Daniudi gas field. The results show that the rock mechanical performances and the acid etching conductivities of the rock specimens are related to the types of reservoirs. The rock mechanical properties can be deteriorated after acidizing, but different types of reservoirs have different degrees of deterioration. According to the results of acid etching conductivity of different types of reservoirs, conductivities obtained by high and low viscosity and cross-link-gelled acid (two stage injection) processes are higher than those of high viscosity systems. The experimental results of process suitability suggest adopting high and low viscidity acid systems for pore type and fracture-dissolved pore type reservoirs, and cross-linked acid systems for fracture-pore type reservoirs. The findings of this study can help form a better understanding of the performance of different types of reservoirs under the various acidified conditions that can be used for the optimization of acid fracturing processes in carbonate formations.

Keywords: Ordos Basin; Majiagou Formation; carbonatite; acid erosion diversion; acid fracturing process

Citation: Zhang, Y.; Mao, H.; Zhang, H.; Li, Y.; Jiang, Y.; Li, J. Optimization of Acid Fracturing Process for Carbonate Reservoirs in Daniudi Gas Field. *Energies* **2022**, *15*, 5998. https://doi.org/10.3390/en15165998

Academic Editors: Reza Rezaee and Pål Østebø Andersen

Received: 22 May 2022
Accepted: 10 August 2022
Published: 18 August 2022

1. Introduction

The Daniudi gas field is located in the northern part of the Yishan slope in the Ordos Basin. The gas-bearing layers are the Carboniferous Taiyuan Formation, the Permian Shanxi

Formation, and the Lower Shihezi Formation. River-like sedimentary sequence [1,2]. The oil and gas exploration of the Ordovician Majiagou Formation in the Daniudi area of the Ordos Basin has continued to make breakthroughs. Practice shows that the Ma5 Member is gas-bearing as a whole, but there are many types of reservoirs and complex genesis. In order to systematically summarize the genetic types of the reservoirs in this section, the type of reservoir space and the main controlling factors for reservoir development were analyzed by means of core observation, thin section identification, cathodoluminescence thin section observation, whole-rock X-ray diffraction analysis, and carbon and oxygen isotope analysis. Research. The results show that the Majiagou Formation reservoirs in the study area develop intercrystalline pores, intercrystalline dissolved pores, micro-fractures, residual intergranular pores, and intragranular dissolved pores [3]. The gas field develops seven sets of main gas layers in the vertical direction. The average porosity of the reservoir is 7.62–10.27%, the average permeability is 0.55×10^{-3}–1.36×10^{-3} μm^2, and the pressure coefficient is 0.8–1.0. It is a typical low-porosity, low-permeability, and low-pressure gas reservoir with low natural productivity and great difficulty in development.

Structurally, the Daniudi gas field can be divided into five sub-members from top to bottom from the Ordovician carbonate weathering crust gas reservoir in the Lower Paleozoic. The inter-subtidal depositional environment is dominated by a set of stable, thick-layered dark gray–gray–black limestone, lime dolomite, and dolomite. The stratum is laterally stable and the thickness variation is small, generally 24~30 m, with an average of 26.8 m. The main reservoir space types are fractures, dissolution expansion pores, and intercrystalline dissolved pores, with a small number of karst caves and fractures and caves developed. The main distribution range of porosity is 1–8%, and the main distribution range of permeability is 0.01–1 mD. Generally, it is characterized by low porosity, tightness, and ultra-low permeability, and a single well generally has no natural productivity [4]. Since 2012, with the help of the horizontal well development method, the production stimulation technologies, such as pre-fluid acid fracturing, compound sand addition acid fracturing, and multi-stage injection + temporary plugging volume acid fracturing, have been gradually optimized, and the development of tight and low-permeability carbonate reservoirs has been achieved [5]. However, the conditions of different types of reservoirs are quite different, and the targeted acid fracturing technology is not matched and imperfect, resulting in large differences in the productivity of different horizontal wells after fracturing and a high proportion of low-yield wells, which cannot meet the economic and effective development of this type of gas reservoir. Therefore, it is necessary to carry out corresponding differential acid fracturing technology research for different types of carbonate reservoirs to further improve the performance of acid fracturing. The general sketch of the problem under study is shown in Figure 1.

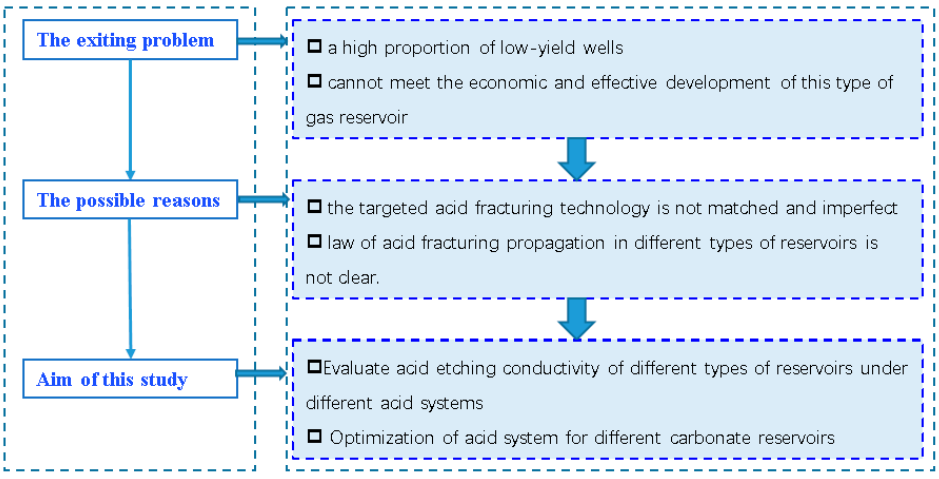

Figure 1. The general sketch of the problem under study.

To optimize the acid fracture process, the first thing to do is to explore the performance of different types of reservoirs in different acid conditions. Acid fracturing, which is a common method to increase the productivity of wells in carbonate reservoirs, has been studied for decades. In the 1970s, Nocotny had already started research and laboratory test work on the conductivity of acid-etched cracks [6]. Malik and Hill [7] designed a method to test the conductivity of acid-etched cracks in 1989. For the first time, the study involves the effect of acid-etched fracture surface morphology on conductivity. Beg et al. [8] pointed out that the deep trenches formed after acid etching cracks can provide greater conductivity, but the overall conductivity of acid etching cracks is also related to the force on the cracks after acid etching. In order to simulate the flow of acid in the formation more realistically, Suleimenov et al. [9] adopted two lithologic rock slab tests. With the rapid development of energy production in carbonate reservoirs, the acid fracturing method has drawn more and more attention [10–12]. Some scholars carried out experimental studies to investigate the deterioration of rock properties [13–15], the acid etching fracturing [16–18], and the fracturing conductivity [19–21]. In addition, some scholars have developed numerical models to simulate the acid fracturing process to analyze the fracture development [12,22] and acid fracture conductivity [23,24]. The effect of the microstructure of the acidification on the micro-properties is another hotspot in acid fracturing research [25–27]. Previous studies showed that the carbonate formation has complex reservoir spaces, which can significantly affect the production rate of carbonate reservoirs [28,29]. At present, although more attention has been paid to the microscopic behavior of acid fracturing in different types of reservoirs, no systemic studies have been carried out for researchers to investigate the effect of reservoir space on the rock mechanical performance and the acid fracturing conductivity.

The acid fracturing process plays a key role in the production rate in carbonate reservoirs. Plenty of studies have been done to investigate acid fracturing construction technology [30,31]. Nelson [32] first used the three-stage alternate injection of 28% HCL + 30 min closing acidification technology in horizontal wells in 1998. Through the field construction curve, it was found that the fracturing pressure of the formation decreased significantly with the continuous increase of the alternating series. Due to the low viscosity of the acid solution, serious filtration loss, and insufficient effective distance of acid corrosion cracks, the actual production capacity did not reach the expected value. In 2012, Dong [33] et al. optimized the injection series through the acid fingering model. Using three-stage alternating injection (20% gelling acid), a gas production of 6.218 million cubic meters per day was obtained in Puguang, setting the highest single-well production at that time. In 2017, Jiang et al. [34] used the orthogonal analysis method to optimize the acid type and the amount of acid injection, and successfully reduced the fracture pressure of the reservoir by using the two-stage alternating injection method in the field. The deep-penetrating acid fracturing process using multi-stage injection has undergone more than 40 years of development [35–37]. From the initial vertical well single-process stimulation to the current composite stimulation method combined with long horizontal well sections, the multi-stage alternate injection acid fracturing process has become more and more mature, and its own applicability to carbonate reservoir stimulation has been proved by production practice [38–40]. To date, production improvement of carbonate reservoirs via optimization of acid fracturing design parameters has been investigated under both laboratory tests and numerical simulations [41]. However, the optimization design of construction parameters based on the reservoir space is seldom analyzed.

This paper aims to explore the effects of acidification on the performance of different types of reservoirs and the acid etching on the conductivity of rock slabs with different reservoir spaces and to optimize the multi-stage acid fracturing process and construction parameters for different types of reservoirs. To do so, firstly, triaxial compression tests have been carried out, and the mechanical properties of rock samples with different reservoir spaces before and after acidification have been compared and analyzed. After that, acid etching conductivity experiments of rock slabs with different types of reservoirs have been conducted under realistic acid conditions to simulate the multi-stage acid fracturing

process. This study contributes to the understanding of the performance of different types of reservoirs under the various acidified conditions, and provides practical guidelines for the optimal construction of acid fracturing in different types of carbonate reservoirs.

2. Analysis of the Effect of Acidification on the Mechanical Properties of Rocks

2.1. Rock Specimens

The rock cores collected in the Daniudi gas field were buried at depths ranging from 3000 m to 3200 m. The rock cores are mainly thick-layered dark gray–gray–black limestone with different reservoir spaces. Carbonate formations could be divided into five types based on the reservoir space: pore type, fractured type, fracture-pore type, fracture-cavern type, and pore-fracture-cavern type. According to the analysis of the characteristics of the cores, the main reservoir space types of the Daniudi gas field are fractures, pores, and fractures and caverns.

In order to reveal the mechanical behavior of different rock formations, rock specimens with different reservoir spaces were prepared for triaxial tests. Rock cores with similar mineral components were selected and cut into cylindrical samples with a size of 25 mm in diameter and 50 mm in height. Based on the results of X-ray diffraction (XRD) testing carried out on the collected rock cores, the mineral contents of the formations are mainly dolomite, calcite, and quartz, as shown in Table 1. The acid etching samples were immersed in 20% HCl for 20 min before the test.

Table 1. Mineral components of rock cores with different reservoir space.

Reservoir Space	Dolomite	Calcite	Quartz
Pores1#	96.77	1.06	2.17
Pores2#	95.59	1.25	3.16
Fractures and caverns1#	96.05	2.86	1.08
Fractures and caverns2#	97.77	1.32	0.91
Fractures and pores1#	97.04	2.45	0.5
Fractures and pores2#	96.31	2.82	0.87

2.2. Testing Equipment and Testing Procedure

In order to study the influence of acidification on the mechanical properties of rocks with different reservoir space, triaxial compression tests were carried out. All experiments were conducted in a high temperature and high pressure triaxial rheological testing machine—XT-01. The experimental process is shown in Figure 2. The experimental device includes an axial pressure system, a lateral pressure system, a pore water pressure system, a temperature control system, and a control system. Axial compression system: maximum axial test force 2000 kN; Maximum working oil pressure 28 MPa; Maximum axial deformation 5.0 mm; Maximum radial deformation 2.5 mm; Maximum piston displacement 100 mm, the measurement accuracy of the above values are 1%. The loading rate of the tests was set 10^{-4} mm/s, and the confining stresses were 10 MPa, 20 MPa, 40 MPa, and 60 MPa.

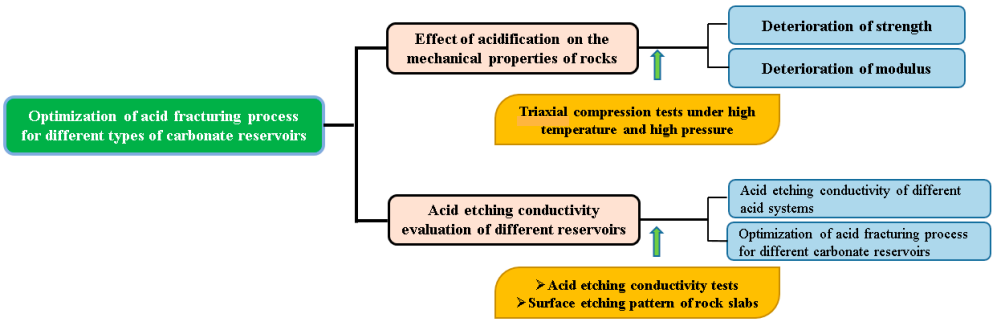

Figure 2. The flowchart of this study.

2.3. Analysis of Acid Etching on the Failure Strength of Rock Samples with Different Reservoir Spaces

In this study, triaxial compression tests were first carried out on the rock samples with different reservoir space types. The mechanical performance of samples of reservoir space types is collected and shown in Figure 3. As illustrated in Figure 3a, the failure strength of samples with different reservoir space types increases with confining stress. It is also found that the rock samples with reservoir space of pores have the highest failure strength, the rock samples with reservoir space of fracture-pores have the lowest failure strength, and the failure strength of a rock sample with reservoir space of space-dissolved pore is between the other two under the same confining stress. The elastic modulus of samples of porous reservoir is much larger than the other two under the same confining stress.

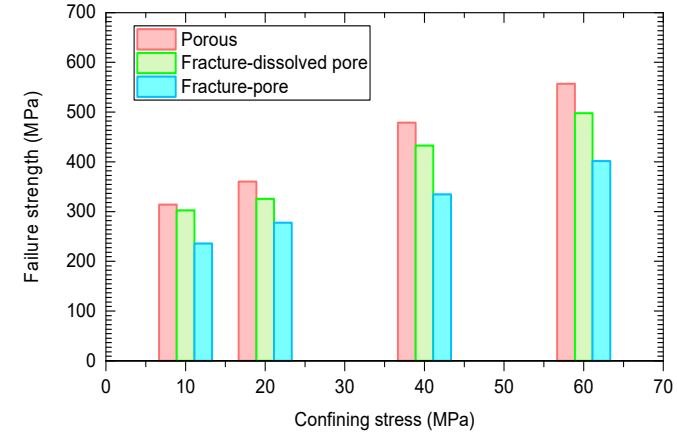

(**a**)

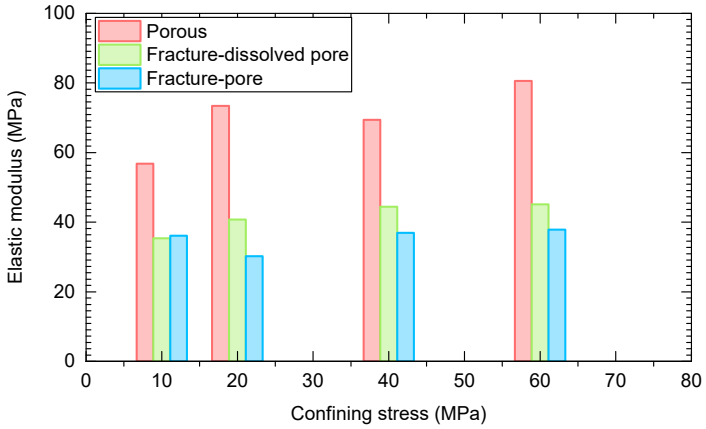

(**b**)

Figure 3. Mechanical behavior of rock samples with different reservoir spaces under triaxial compression conditions: (**a**) failure strength; (**b**) Elastic modulus.

To explore the effect of acid etching on the strength of samples with different reservoir types, traxial compression tests on the rock samples after acid etching were also carried out. The failure strength of rock samples before and after acid etching was compared and demonstrated in Figure 4. It is indicated that the failure strength of all the samples decreases after being treated by acid etching. For example, the failure strength of original rock samples with fracture-dissolved pore under a confining stress of 40 MPa is 433.1 MPa, while the failure strength is reduced to 264.2 MPa after acidifying with a reduction of 39.0%. It is also clear that rock samples with different reservoir types have different reductions in the failure strength. Reductions of the failure strength of different rock samples demonstrated in Figure 5 show that the reduction in the failure strength is related to the reservoir space type. Samples with the reservoir space of fracture-dissolved pore have the highest reduction, ranging from 35.5 %

to 44.7 %, while samples with pore have the lowest reduction ranging from 11.2% to 25.9%, and the reduction of samples with fracture pore is between 27.9% and 39.2%.

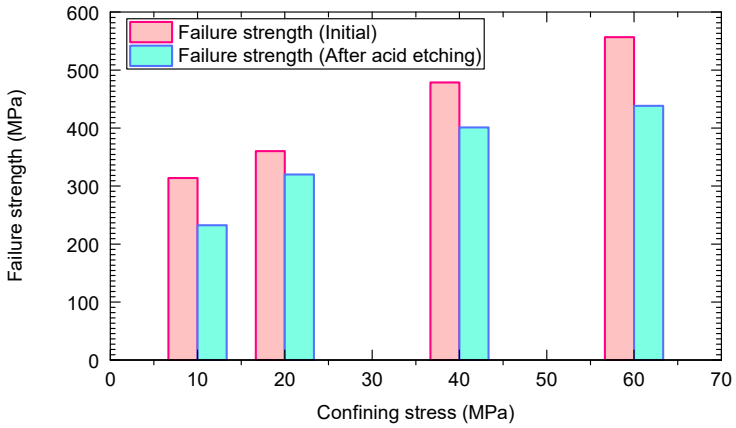

(**a**)

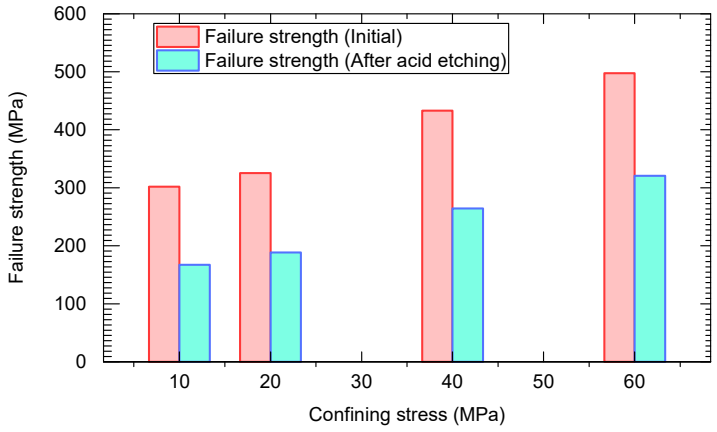

(**b**)

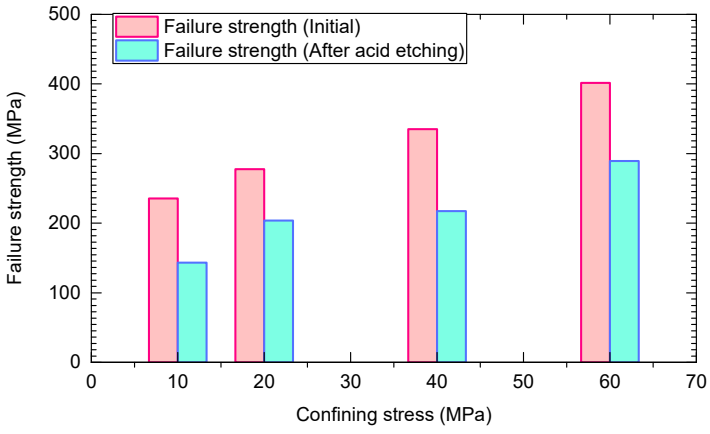

(**c**)

Figure 4. Effect of acid etching on the failure strength of rock samples with different reservoir space: (**a**) Porous, (**b**) Fracture-dissolved pore, (**c**) Fracture-pore.

The effects of the acid etching on the elastic modulus of different types of rock samples are illustrated in Figure 6. After acid etching, all samples show a reduction of the elastic modulus, while different types of rock samples have different degrees of decline. Basically, the rock samples of the fracture-dissolved pore type have a very high decrease, and the

elastic modulus reduction of the other two types of rock samples is relatively small, as illustrated in Figure 7.

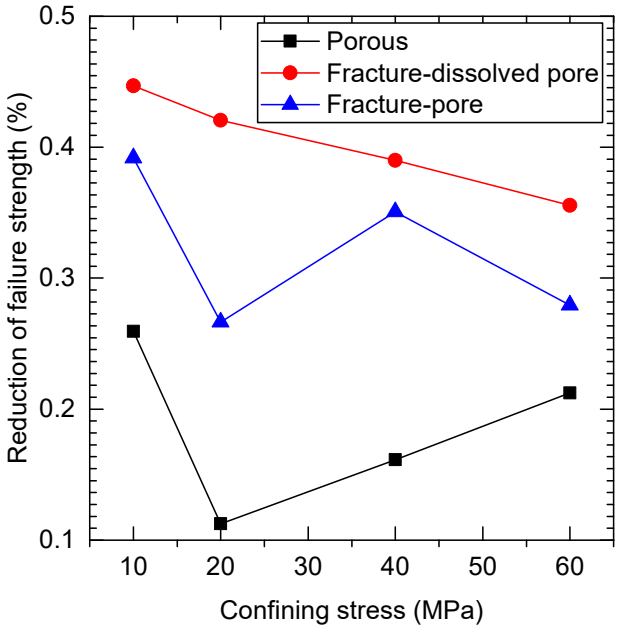

Figure 5. Failure strength reduction of rock samples with different reservoir spaces.

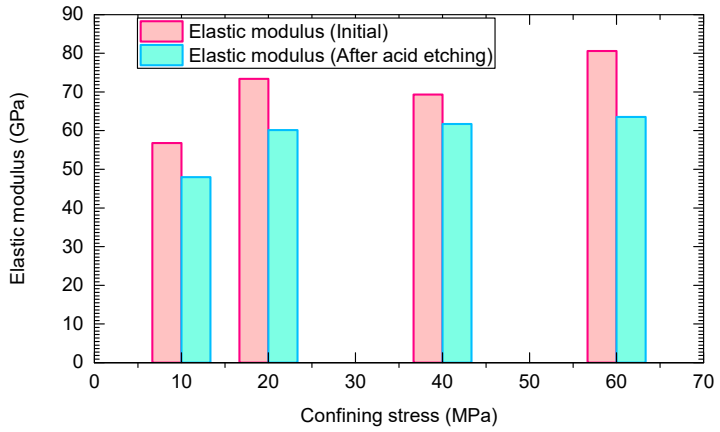

(**a**)

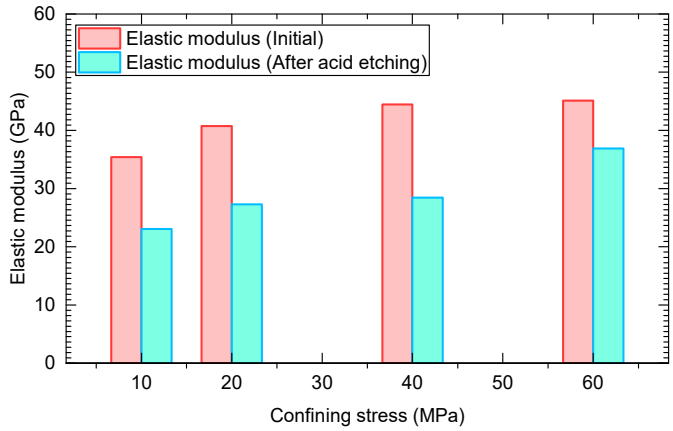

(**b**)

Figure 6. *Cont.*

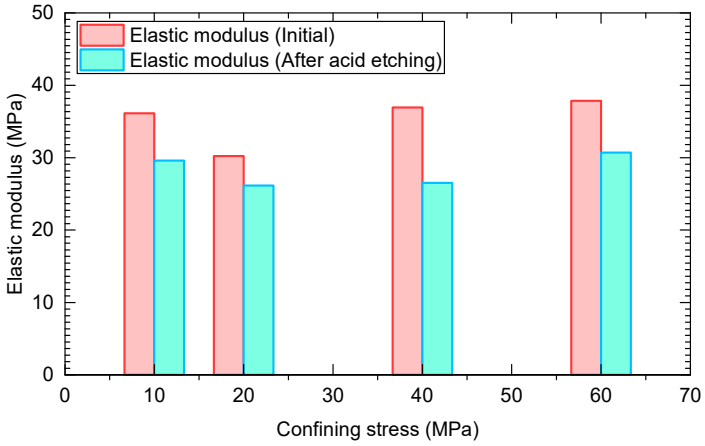

(**c**)

Figure 6. Effect of acid etching on the elastic modulus of rock samples with different reservoir space: (**a**) Porous, (**b**) Fracture-dissolved pore, (**c**) Fracture-pore.

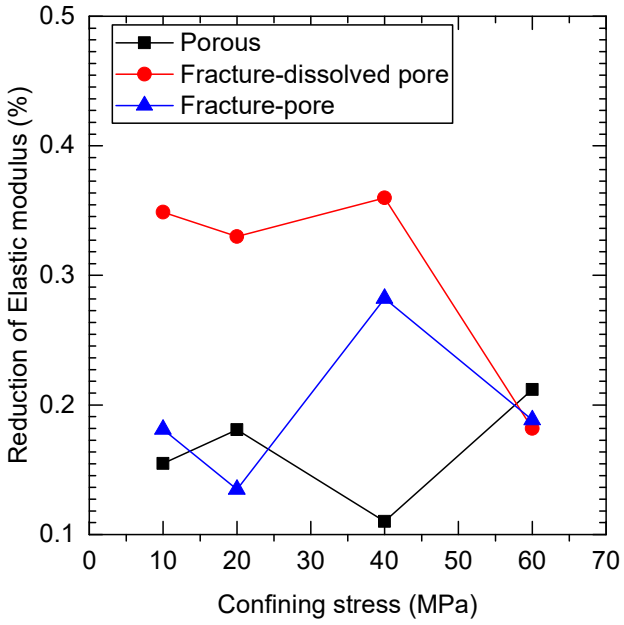

Figure 7. Elastic modulus reduction of rock samples with different reservoir space.

3. Experimental Program of Acid Etching Conductivity Experiment

In order to explore the effect of acid etching on the conductivity behavior of the carbonate formations with different space types, the acid etching fracture experiments have been conducted. The rock slabs with a size of 17.7 cm long (with semi-circular arcs with a diameter of 38 mm at both ends), 3.8 cm wide, and 1.5–2.5 cm thick were prepared and shown in Figure 8, and the properties of the rock slabs are listed in Table 2.

Table 2. The preferred experimental scheme for different acid fracturing processes for three different reservoir types.

No.	Type Well	Type	Well No.	Layer	Depth (m)	Acid Type
1	4 17/82	fracture-pore	D1-530	MaWu5	3120.12–3120.34	High and low viscous acid (secondary injection)
	4 17/82	fracture-pore	D1-530	MaWu5	3120.12–3120.34	
2	4 26/123-1	fracture-pore	DK13-FP8	MaWu5	3002.86–3003.08	Cross-linked acid (secondary injection)
	4 26/123-2	fracture-pore	DK13-FP8	MaWu5	3002.86–3003.08	
3	6 47/82-1	fracture-pore	DK13-FP8	MaWu6-7	3041.04–3041.27	High Viscose Gel
	6 47/82-2	fracture-pore	DK13-FP8	MaWu6-7	3041.04–3041.27	

Table 2. *Cont.*

No.	Type Well	Type	Well No.	Layer	Depth (m)	Acid Type
4	8 35/165-1	fracture-cavern	DK13-FP8	MaWu6-7	3052.08–3052.3	High Viscose Gel
	8 35/165-2	fracture-cavern fracture-cavern	DK13-FP8	MaWu6-7	3052.08–3052.3	
5	10 8/49-1	fracture-cavern	DK13-FP8	MaWu6-7	3064.15–3064.36	Cross-linked acid (secondary injection)
	10 8/49-2	fracture-cavern	DK13-FP8	MaWu6-7	3064.15–3064.36	
6	10 14/49-1	fracture-cavern	DK13-FP8	MaWu6–7	3065.12–3065.32	High and low viscous acid (secondary injection)
	10 14/49-2	fracture-cavern	DK13-FP8	MaWu6-7	3065.12–3065.32	
7	4 59/123-1	porous	DK13-FP8	MaWu5	3007.39–3007.64	High and low viscous acid (secondary injection)
	4 59/123-2	porous	DK13-FP8	MaWu5	3007.39–3007.64	
8	4 36/67-1	porous	DK13-FP8	MaWu5	3008.54–3008.75	Cross-linked acid (secondary injection)
	4 36/67-2	porous	DK13-FP8	MaWu5	3008.54–3008.75	
9	6 59/82-1	porous	DK13-FP8	MaWu6-7	3043.18–3043.41	High Viscose Gel
	6 59/82-2	porous	DK13-FP8	MaWu6-7	3043.18–3043.41	

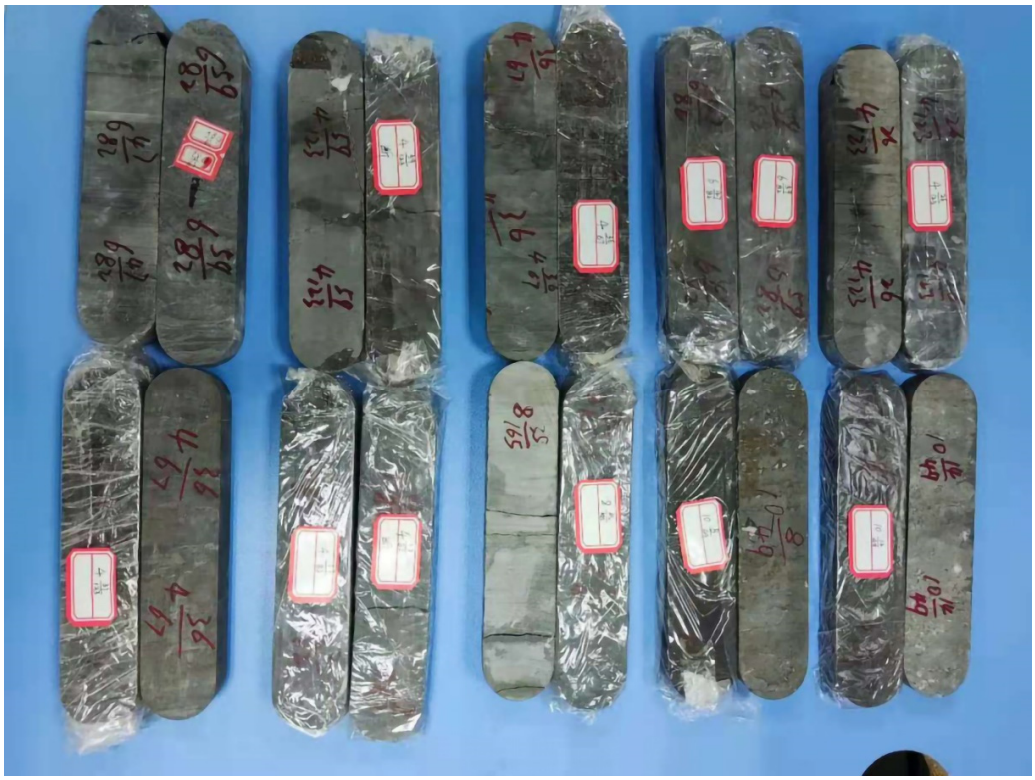

Figure 8. Rock slabs for acid etching tests.

3.1. Acidizing Fluids

The objective of this study is to optimize the acid fracturing process and construction parameters and to develop corresponding differentiated acid fracturing technology for carbonate formations with different pore types. To do so, the acid etching conductive test was conducted on rock slabs of different pore types in three acid formulas. The acid formulas are shown as follows.

(1) High viscosity acid formula: 20% HCl + 1.0% corrosion inhibitor + 0.2% iron ion stabilizer + 0.2% drainage aid + 0.45% thickener;
(2) Low-viscosity acid formula: 20% HCl + 1.0% corrosion inhibitor + 0.2% iron ion stabilizer + 0.2% drainage aid + 0.15% thickener;
(3) Cross-linked acid formula: 20% HCl + 1.0% corrosion inhibitor + 0.2% iron ion stabilizer + 0.2% drainage aid + 0.45% thickener + cross-linking agent A:B = 100:0.6, cross-linking. The ratio is 100:0.3.

3.2. Experimental Method and Process

The acid etching conductivity experimental instrument includes three parts: the acid etching experimental system, the fracturing propagation conductivity test system, and the slate scanning system, as shown in Figure 9. The acid etching experimental device adopts the HXDL-2C acid etching crack conductivity analysis test device independently developed by Changjiang University. According to the two test stages of the acid etching crack conductivity experiment, the experimental equipment is divided into two parts: the acid etching experimental device and the crack conductivity test device. The acid etching experiment refers to placing the rock slab that meets the API standard in the API diversion chamber, maintaining a certain opening between the walls of the rock slab to simulate formation cracks, and using an acid-resistant pump to pump the prepared acid from the liquid storage tank into the diversion. In the room, the acid reacts with the rock when it flows on the fracture wall, which can approximate the real situation of the acid–rock reaction in the acid fracturing construction. The slate scanning system is the EinScan Pro2X Plus 3D laser scanner from Hangzhou Xinglin 3D. Through 3D laser scanning, it can quantitatively analyze the degree of corrosion of the rear face of acid etching of fractures and explain the reasons for the differences in acid erosion diversion from a microscopic point of view.

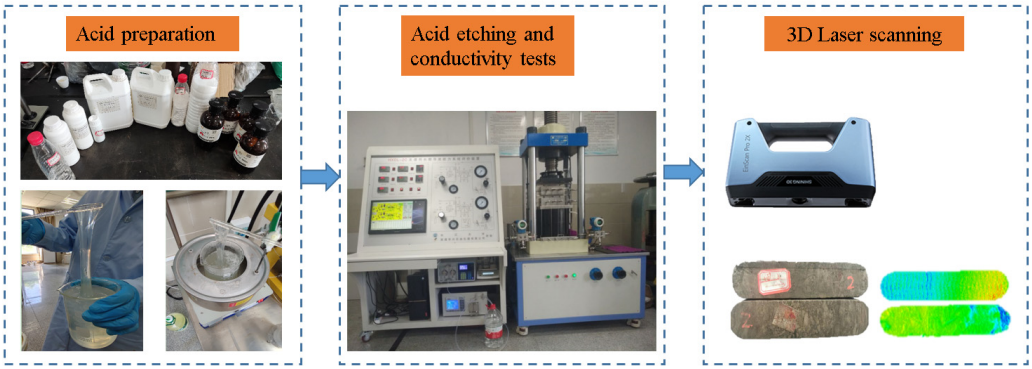

Figure 9. Acid etching conductivity test system.

The main purpose of the acid-etched fracture conductivity testing system is to increase the simulation scale of the experimental research and make the experimental conditions as close to the field conditions as possible. Through the motion similarity criterion, the on-site acid injection displacement was converted to the laboratory experimental displacement, and the acid injection displacement was determined to be 40 mL/min, and the acid-rock reaction time was 90 min. The crack width between the rock slabs is controlled at 1 mm, and the back pressure valve is controlled at 7.6 MPa during the acid-rock reaction, so that the generated CO_2 is dissolved in the liquid to avoid the two-phase flow affecting the acid-rock reaction.

3.3. Experimental Steps

According to the test method recommended in the oil and gas industry standard SY-T 6302–2009 "Recommended method for short-term conductivity evaluation of fracturing proppant packs", the conductivity test of acid-etched fractures and sand was carried out. During the acid etching experiment, corrosive acid is injected into the crack under high temperature and high pressure conditions, so the experimental operation must first be safe. The main experimental steps are as follows:

(1) Before the acid-rock reaction, all cores are marked with front and back and high-precision scanning of the surface.
(2) Weighing. Before the experiment, the experimental slate was weighed, and the acid solution used in the experiment was prepared according to the on-site formula.

(3) Put the experimental rock slabs into the diversion chamber of the acid-etched diversion capacity evaluation equipment, lay proppant between the two rock slabs to simulate the gap width, and seal them with high-temperature resistant silica gel.
(4) Connect relevant pipelines, inject saturated standard brine by vacuuming, heat the reaction system, wait for the experimental temperature to reach 100 °C, start injecting acid solution with a fixed displacement of 40 mL/min and a back pressure of 7 MPa, and carry out acid etching experiments on rock slabs.
(5) After the reaction is over, take out the slate, take pictures and weigh after cleaning, scan the acid-rock reaction surface and clean the instrument.
(6) Put the acid-etched experimental rock slab into the diversion chamber to measure the short-term diversion capacity under different closing pressures.
(7) After the experiment is completed, disassemble the device and clean up the relevant experimental equipment.
(8) Stop running the computer experimental program, export the experimental data, and organize the experimental report.

3.4. Analysis of Experimental Results

3.4.1. Influence of Different Acid Pressing Processes on Etching Morphology

In order to evaluate the effect of the acid etching on rock samples with different reservoir space types, the surface morphology of rock samples after acidification has been scanned by a 3D laser scanner and analyzed by Surface software. Figure 10 illustrates the etching features of different types of rock samples.

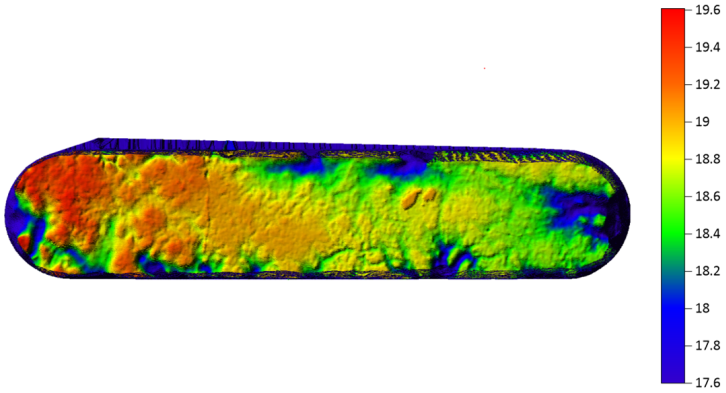

(**a**)

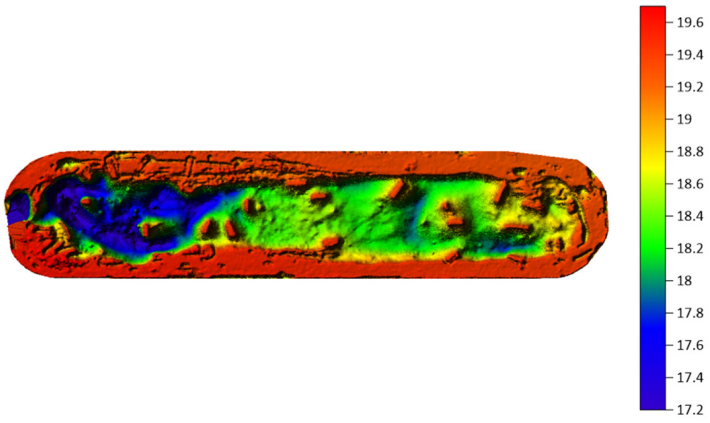

(**b**)

Figure 10. *Cont.*

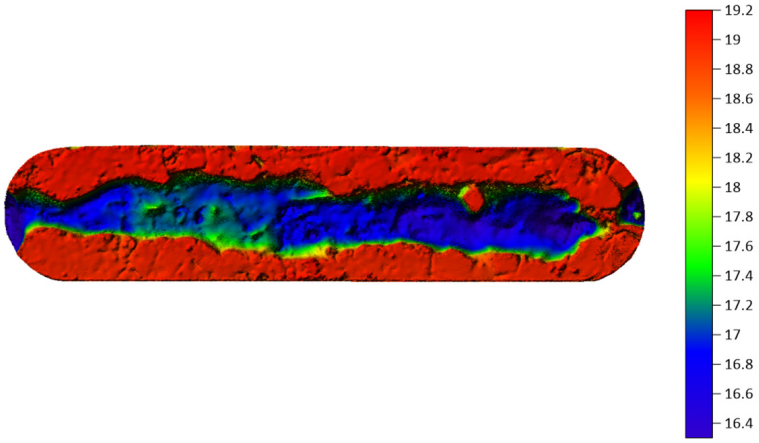

(**c**)

Figure 10. Characterization of the surface morphology of different slates after acid etching (**a**) pore type; (**b**) fracture-cavern type; (**c**) fracture-pore type.

The surface etching of rock samples with pore type is a typical rough etching pattern, as shown in Figure 10a. The mass change of the upper and lower rock plates of the pore type reservoir after acid etching i is relatively small. The acid etching effect at the entrance is more obvious, and the concavity is uneven. There are some acid etching holes in the middle, but they are not continuous.

The surface etching of rock samples with fracture-cavern type and fracture-pore type is a typical channel etching pattern, as shown in Figure 10b,c. The quality of the upper and lower slabs of the fracture pore type reservoir after acid etching is relatively greater than that of the pore type. The acid etching effect of the pore type reservoir is relatively continuous, and the entrance end is a bit deeper with a continuous acid etching section, as shown in Figure 10b.

After acid etching, the mass of the upper and lower rock slabs of the fracture-cavern type reservoir changes the most. The acid etching effect of the whole rock slab of the fracture-cavern type reservoir is more continuous, the corrosion of the rock plate is more serious, and the export of liquid is fast. The acid etching generated a lot of gas during the testing process, and the residual acid block has a lot of tiny particles.

3.4.2. Analysis of the Conductivity of Different Acid Fracturing Processes

The acid corrosion conductivity were calculated by the calculation model proposed by API.RP6 [42], the calculation formula of acid corrosion conductivity is:

$$kW_f = 5.555\, Q\mu/\Delta p \tag{1}$$

where k is the acid etching conductivity, $\mu m^2 \cdot cm$, W_f is the crack width, cm, μ is the liquid viscosity, mPa·s, Q is the liquid flow, mL/min, and Δp is the differential pressure in the draft chamber, MPa.

Through three different acid fracturing processes and three different types of rock slabs, acid erosion conductivity experiments are carried out, and the experimental results are used for analysis. A comparison of the conductivity curves of different types of reservoirs under different process conditions is shown in Figures 11–13.

It can be seen from the conductivity maps of fracture-porous reservoirs under different closing pressures in Figure 11 that the conductivity of high-low viscosity and cross-linked acid is larger than that of high-viscosity acid processes. The fingering effect and the difference in the reaction rates of high and low viscous acids enhance the non-uniform etching effect of fractures and improve fracture conductivity; at the same time, low-viscosity acid is conducive to the reconstruction of smaller-scale natural fractures and dissolved

pores, and promotes the improvement of fracture complexity and the expansion of the transformation volume.

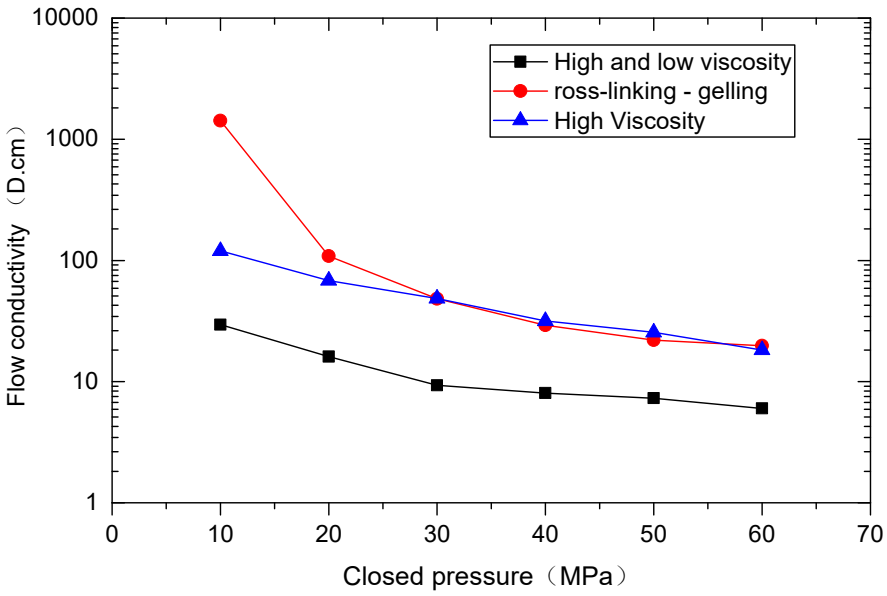

Figure 11. Conductivity of fracture-pore reservoirs under different closing pressures.

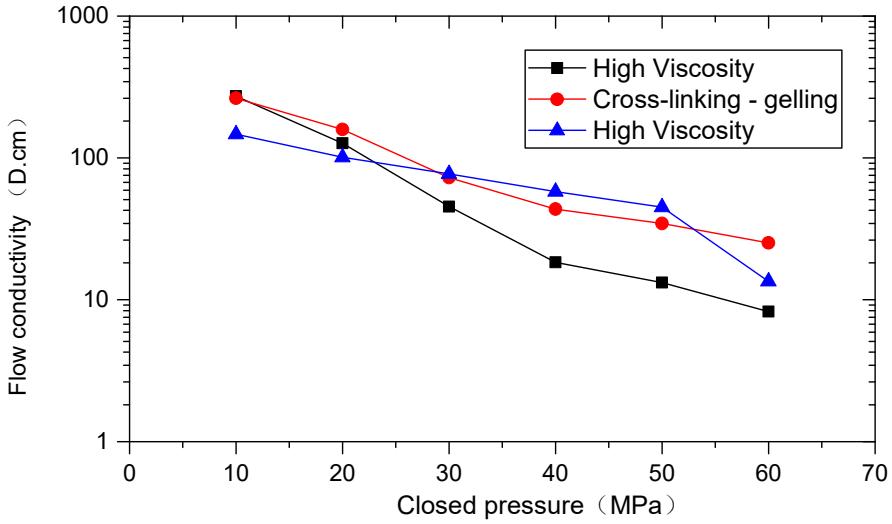

Figure 12. Conductivity of fracture-dissolved pore reservoirs under different closing pressures.

From the perspective of the conductivity of fracture-dissolved pore reservoirs under different closing pressures in Figure 12, the conductivity of cross-linking fluid + gelling acid is the highest. Considering the use of the strong penetration performance of low-viscosity liquids to communicate natural fractures, it is preferable to use a linear glue + gelling acid system for multi-stage alternating injection of liquids.

Judging from the conductivity of pore-type reservoirs under different closing pressures in Figure 13, the high-low viscosity and cross-linking fluid + gelling acid systems have little difference, and the effect of multi-stage injection is stronger than that of the high-viscosity process alone. The multi-stage injection sand acid fracturing technology combines the deep penetration mechanism with the principle of sand fracturing to create high-conductivity fractures. Through the multi-stage injection of fracturing fluid and gelling acid, the reaction rate of acid rock is reduced and the fractures are accelerated. Front extension; in the later stage, the proppant is carried into the formation by the fracturing fluid, which ensures the long-term high conductivity of the fracture.

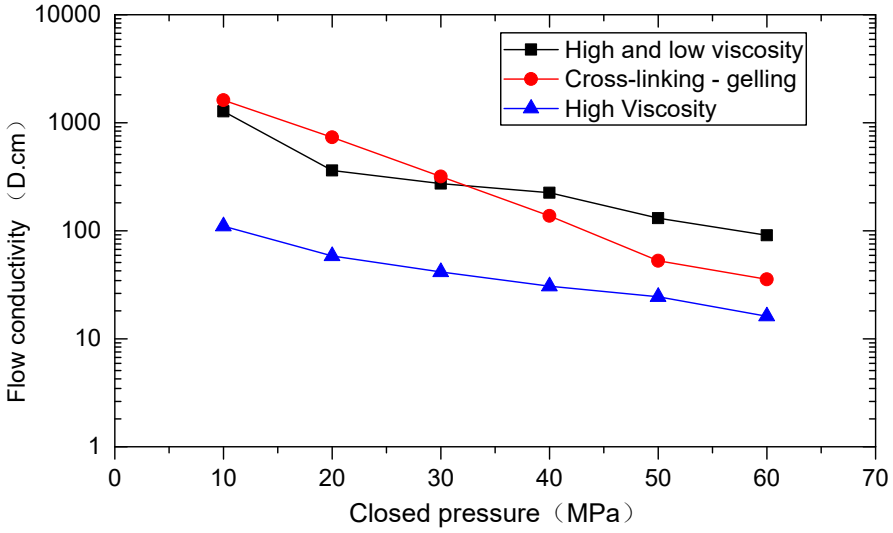

Figure 13. Conductivity of porous reservoirs under different closing pressures.

4. Summary and Conclusions

In this paper, laboratory-based experimental studies on the effect of acidification on the mechanical behavior of rock specimens with different reservoir spaces have been conducted. Acid fracturing conductivity of rock slabs of different types of carbonate reservoirs under various realistic acid conditions has also been investigated to optimize the design of acid fracturing in different reservoirs. The main conclusion has been drawn as follows:

1. The mechanical properties of all rock samples are weakened after acidification, but the degrees of weakening of samples differ with different reservoir spaces. The failure strength of acidified rock is porosity type > fracture-cavern type > fracture − pore type, and the reduction of the elastic modulus of acidified rock is fracture-cavern type > fracture − pore type > porosity type.
2. From the results of acid-etching conductivity of rock slabs for different types of reservoirs, the difference in conductivity capacity of rock slabs after different acid compression processes is large, but the acid-etching conductivity shows a rapid decreasing trend as the closure stress increases. The infusion capacity obtained by the high and low viscosity and cross-linked-gelatinized acid (secondary injection) processes is higher than that of the high viscosity system.
3. From the results of process suitability experiments, high and low viscosity acid systems are recommended for pore type and fracture-solution pore type reservoirs, and cross-linked acid systems are recommended for fracture-pore type reservoirs.

This study carried out acid etching tests considering realistic process under different acid conditions, and the results can provide guideline for the production in different types of reservoirs. It should be noted that the acid etching conductivity test is conducted under one-direction compression, and the fluid flows in a plane. However, in realistic conditions, the stress field is 3-dimensional, and the acid flows are spatial. Therefore, further studies under true triaxial conditions are needed.

Author Contributions: Conceptualization, Y.Z. and H.M.; methodology, H.Z.; formal analysis, Y.L.; investigation, Y.J. and J.L.; resources, Y.J.; data curation, J.L.; writing—original draft preparation, Y.Z.; writing—review and editing, H.M. and H.Z.; visualization, J.L.; supervision, H.M.; project administration, Y.Z. All authors have read and agreed to the published version of the manuscript.

Funding: This research received no external funding.

Conflicts of Interest: The authors declare no conflict of interest.

Nomenclature

k	acid etching conductivity, $\mu m^2 \cdot cm$;
W_f	crack width, cm;
μ	liquid viscosity, mPa·s;
Q	liquid flow, mL/min;
Δp	differential pressure in the draft chamber, MPa.

References

1. Liu, M.; Ding, X.; Wan, Y.; Bai, X.L.; Chen, Q.Q.; Le, J.P. Characteristics and distribution of Ordovician weathering crust reservoirs in Daniudi gas field, Ordos Basin. *Mar. Orig. Pet. Geol.* **2014**, *19*, 35–42.
2. Yang, H.; Fu, J.H.; Wei, X.S.; Ren, J.F. Natural gas exploration domains in Ordovician marine carbonates, Ordos Basin. *Acta Pet. Sin.* **2011**, *32*, 733–740.
3. He, J.; Fang, S.; Hou, F.; Yan, R.; Zhao, Z.; Yao, J.; Tang, X.; Wu, G. Vertical zonation of weathered crust ancient karst and reservoir evaluation and prediction—A case study of M55–M51 sub-members of Majiagou Formation in gas fields, central Ordos Basin, NW China. *Pet. Explor. Dev.* **2013**, *40*, 572–581. [CrossRef]
4. Zhang, L.; Gao, X.; Liu, M.; Li, J.; Shi, Y.; Su, Z. Assessment about the tight carbonate reservoir of the fifth submember of member Ma-5 in Lower Ordovician of Ordos Basin. *Pet. Geol. Oilfield Dev. Daqing* **2018**, *37*, 16–21.
5. Li, K.; Xu, B.; Qin, Y.; He, Q. Study on diversion acid technology in tight carbonatite gas reservoir. *J. Southwest Pet. Univ. Sci. Technol. Ed.* **2013**, *35*, 97–101.
6. Nocotny, E.J. Prediction of stimulation from acid fracturing treatments using finite fracture conductivity. *J. Pet. Technol.* **1977**, *29*, 1186–1194. [CrossRef]
7. Malik, M.A.; Hill, A.D. A new technique for laboratory measurement of acid fracture conductivity. In Proceedings of the SPE Annual Technical Conference and Exhibition, San Antonio, TX, USA, 8–11 October 1989.
8. Beg, M.S.; Kunak, A.O.; Gong, M.; Zhu, D.; Hill, A.D. A systematic experimental study of acid fracture conductivity. *SPE Prod. Oper.* **1996**, *13*, 267–271. [CrossRef]
9. Suleimenova, A.; Zhu, D. Comparative Study of Acid Hydraulic Fracturing and Propped Hydraulic Fracturing for a Tight Carbonate Formation. In Proceedings of the 78th EAGE Conference, Vienna, Austria, 30 May–2 June 2016.
10. Zhukov, V.S.; Kuzmin, Y.O. Experimental evaluation of compressibility coefficients for fractures and intergranular pores of an oil and gas reservoir. *J. Min. Inst.* **2021**, *251*, 658–666. [CrossRef]
11. Adewunmi, A.A.; Solling, T.; Sultan, A.S.; Saikia, T. Emulsified acid systems for oil well stimulation: A review. *J. Pet. Sci. Eng.* **2022**, *208*, 109569. [CrossRef]
12. Qi, N.; Chen, G.; Pan, L.; Cui, M.; Guo, T.; Yan, J.; Liang, C. Numerical simulation and analysis of fracture etching morphology during acid fracturing of dolomite reservoirs. *Chem. Eng. Sci.* **2021**, *229*, 116028. [CrossRef]
13. Zhang, H.; Zhong, Y.; Zhang, J.; Zhang, Y.; Kuang, J.; Yang, B. Experimental research on deterioration of mechanical properties of carbonate rocks under acidified conditions. *J. Pet. Sci. Eng.* **2020**, *185*, 106612. [CrossRef]
14. Kang, Q.; Chen, L.; Valocchi, A.J.; Viswanathan, H.S. Pore-scale study of dissolution-induced changes in permeability and porosity of porous media. *J. Hydrol.* **2014**, *517*, 1049–1055. [CrossRef]
15. Lu, C.; Bai, X.; Luo, Y.; Guo, J. New study of etching patterns of acid-fracture surfaces and relevant conductivity. *J. Pet. Sci. Eng.* **2017**, *159*, 135–147. [CrossRef]
16. Gou, B.; Ma, Y.; Liu, Z.; Zhou, C.; Wang, K. Research progress and prospect of numerical modeling for acid fracturing of heterogeneous carbonate reservoirs. *Nat. Gas Ind.* **2019**, *39*, 87–98.
17. Gou, B.; Guan, C.; Li, X.; Ren, J.; Zeng, J.; Wu, L.; Guo, J. Acid-etching fracture morphology and conductivity for alternate stages of self-generating acid and gelled acid during acid-fracturing. *J. Pet. Sci. Eng.* **2021**, *200*, 108358. [CrossRef]
18. Aljawad, M.S.; Aljulaih, H.; Mahmoud, M.; Desouky, M. Integration of field, laboratory, and modeling aspects of acid fracturing: A comprehensive review. *J. Pet. Sci. Eng.* **2019**, *181*, 106158. [CrossRef]
19. Wu, H.-L.; Du, Y.-J.; Yu, J.; Yang, Y.L.; Li, V.C. Hydraulic conductivity and self-healing performance of engineered cementitious composites exposed to acid mine drainage. *Sci. Total Environ.* **2020**, *716*, 137095. [CrossRef]
20. Asadollahpour, E.; Baghbanan, A.; Hashemolhosseini, H.; Motharami, E. The etching and hydraulic conductivity of acidized rough fractures. *J. Pet. Sci. Eng.* **2018**, *166*, 704–717. [CrossRef]
21. Liu, F.; Ma, H.; Li, L.; Zhou, C.; Luo, Z.; Gao, X.; Wu, y. Acid-etched fracture length and conductivity experiments with relayed large-scale rock plates. *J. Pet. Sci. Eng.* **2021**, *196*, 107978. [CrossRef]
22. Furui, K.; Burton, R.C.C.; Burkhead, D.W.; Abdelmalek, N.A.; Hill, A.D.; Zhu, D.; Nozaki, M. A Comprehensive Model of High-Rate Matrix-Acid Stimulation for Long Horizontal Wells in Carbonate Reservoirs: Part I—Scaling Up Core-Level Acid Wormholing to Field Treatments. *SPE J.* **2012**, *17*, 271–279. [CrossRef]
23. Deng, J.; Mou, J.; Hill, A.D.; Zhu, D. A new correlation of acid-fracture conductivity subject to closure stress. *SPE Prod. Oper.* **2012**, *27*, 158–169. [CrossRef]
24. Luo, Z.; Zhang, N.; Zhao, L.; Zeng, J.; Liu, P.; Li, N. Interaction of a hydraulic fracture with a hole in poroelasticity medium based on extended finite element method. *Eng. Anal. Bound. Elem.* **2020**, *115*, 108–119. [CrossRef]

25. Galkin, S.V.; Martyushev, D.A.; Osovetsky, B.M.; Kazymov, K.P.; Song, H. Evaluation of void space of complicated potentially oil-bearing carbonate formation using X-ray tomography and electron microscopy methods. *Energy Rep.* **2022**, *8*, 6245–6257. [CrossRef]
26. Ponomarev, A.; Zavatsky, M.; Nurullina, T.; Kadyrov, M.A.; Galinsky, K.A.; Tugushev, O.A. Application of core X-ray micro-tomography in oilfield geology. *Georesources* **2021**, *23*, 34–43. [CrossRef]
27. Cao, C.; Zhou, F.; Cheng, L.; Liu, S.; Lu, W.; Wang, Q. A comprehensive method for acid diversion performance evaluation in strongly heterogeneous carbonate reservoirs stimulation using CT. *J. Pet. Sci. Eng.* **2021**, *203*, 108614. [CrossRef]
28. Zhang, R.; Hou, B.; Zhou, B.; Liu, Y.; Xiao, Y.; Zhang, K. Effect of acid fracturing on carbonate formation in southwest China based on experimental investigations. *J. Nat. Gas Sci. Eng.* **2020**, *73*, 103057. [CrossRef]
29. Li, Y.; Kang, Z.; Xue, Z.; Zheng, S. Theories and practices of carbonate reservoirs development in China. *Pet. Explor. Dev.* **2018**, *45*, 712–722. [CrossRef]
30. Azad, M.; Ghaedi, M.; Farasat, A.; Parvizi, H.; Aghaei, H. Case study of hydraulic fracturing in an offshore carbonate oil reservoir. *Pet. Res.* **2021**, *in press*. [CrossRef]
31. Thanh, H.V.; Sugai, Y.; Nguele, R.; Sasaki, K. Integrated workflow in 3D geological model construction for evaluation of CO_2 storage capacity of a fractured basement reservoir in Cuu Long Basin, Vietnam. *Int. J. Greenh. Gas Control.* **2019**, *90*, 102826. [CrossRef]
32. Nelson, R.L.; Dyck, W.C.; Jamieson, F.M.; Jenkins, R.A. Multiple Pad-Acid Fraces in a Deep Horizontal Well. In Proceedings of the SPE Rocky Mountain Regional/Low-Permeability Reservoirs Symposium, Denver, CO, USA, 5–8 April 1998.
33. Dong, W.; Xu, X.; Yang, J. Multi-stage alternate injection closed acid fracturing technology and its application in Puguang Gas Field. *Oil Gas Geol. Recovery* **2012**, *19*, 108–110.
34. Jiankun, L.; Tingxue, J.; Chunfang, W.; Youyu, W.; Shihua, L. Alternate acid injection fracturing technology in tight sandstone. *Spec. Oil Gas Reserv.* **2017**, *24*, 150–155.
35. Reza, G.; Sadeqi-Moqadam, M.; Riahi, S. Experimental and Theoretical Studies on the Porous Media Zeta Potential in Mineral Particle Mixtures. *SPE Res. Eval. Eng.* **2021**, *24*, 440–449.
36. Guo, Y.T.; Yang, C.H.; Mao, H.J.; Chen, J.H.; Luo, Y. The characteristics of rock mechanics and acoustic wave parameters of carbonate rock in the north-east Sichuan. *Geochem. Geophys. Geosystems* **2012**, *26*, 471–488.
37. Bawden, W.F. Rock Mechanics Conference Invited Presentation Thoughts on Quantitative Field Scale Characterization of Post-failure Rock Mass Conditions and Their Influence on Underground Mine Design. In Proceedings of the 44th U.S. Rock Mechanics Symposium and 5th U.S.-Canada Rock Mechanics Symposium, Salt Lake City, UT, USA, 27–30 June 2010.
38. Giuffrida, D.; Toribio, E.M.; Murillo, E. First complete quali-quantitative carotenoids characterization of Aiphanes aculeata, Quararibea cordata and Garcinia intermedia fruits. *Appl. Food Res.* **2022**, *2*, 100045. [CrossRef]
39. Tang, H.; An, S.; Zhen, H.; Chen, F. Characterization of combinatorial histone modifications on lineage-affiliated genes during hematopoietic stem cell myeloid commitment. *Acta Biochim. Biophys. Sin.* **2014**, *46*, 894–901. [CrossRef]
40. Ashena, R.; Aminzadeh, F.; Khoramchehr, A. Production Improvement via Optimization of Hydraulic Acid Fracturing Design Parameters in a Tight Carbonate Reservoir. *Energies* **2022**, *15*, 1947. [CrossRef]
41. Ba, N.T.; Thanh, H.V.; Sugai, Y.; Sasaki, K.; Nguele, R.; Quang, T.P.H.; Bao, M.L.; Hai, N.L.N. Applying the hydrodynamic model to optimize the production for crystalline basement reservoir, X field, Cuu Long Basin, Vietnam. *J. Pet. Explor. Prod. Technol.* **2020**, *10*, 31–46.
42. *API-RP 61*; Recommended Practices of Evaluating Short Term Proppant Used in Hydraulic Fracturing Operations. American Petroleum Institute (API): Washington, DC, USA, 1989.